

# 1 Comparison of CSES ionospheric RO data with COSMIC measurements

2 Xiuying Wang<sup>1</sup>, Wanli Cheng<sup>2</sup>, Zihan Zhou<sup>1</sup>, Song Xu<sup>1</sup>, Dehe Yang<sup>1</sup>, Jing Cui<sup>1</sup>

3 1. Institute of Crustal Dynamics, China Earthquake Administration, Beijing, China

4 2. Xinyang Station, Henan Earthquake Administration, Henan, China

5 Corresponding author: Xiuying Wang (652383915@qq.com)

6  
7 **Abstract:** CSES (China Seismo-Electromagnetic Satellite) is a newly launched electric-magnetic  
8 satellite in China. A GNSS occultation receiver (GOR) is installed on the satellite to retrieve electron  
9 density related parameters. In order to validate the radio occultation (RO) data from GOR onboard  
10 CSES, a comparison between CSES RO and the co-located COSMIC RO data is conducted to check  
11 the consistency and reliability of the CSES RO data using measurements from February 12, 2018 to  
12 March 31, 2019. CSES RO peak values ( $N_mF_2$ ), peak heights ( $h_mF_2$ ), and electron density profiles  
13 (EDPs) are compared with corresponding COSMIC measurements in this study. The results show  
14 that: (1)  $N_mF_2$  between CSES and COSMIC is in extremely good agreement with a correlation  
15 coefficient of 0.9898. The near zero bias between the two sets is  $0.005363 \times 10^5 / \text{cm}^3$  with a RMSE  
16 of  $0.3638 \times 10^5 / \text{cm}^3$ ; and the relative bias is 1.97% with a relative RMSE of 16.17%, which are in  
17 accordance with previous studies according to error propagation rules. (2)  $h_mF_2$  between the two  
18 missions is also in very good agreement with a correlation coefficient of 0.9385; the mean difference  
19 between the two sets is 0.59km with a RMSE of 12.28 km, which is within the error limits of  
20 previous studies; (3) Co-located EDPs between the two sets are generally in good agreements, but  
21 with a better agreement for data above 200km than that below this altitude. Data at the peak height  
22 ranges show the best agreement, and then data above the peak regions; data below the peak regions,  
23 especially at the altitude of about the E layer, show relatively large fluctuations. It is concluded that  
24 CSES RO data are in good agreement with COSMIC measurements, and the CSES RO data are  
25 applicable for most ionospheric-related studies considering the wide acceptance and application of  
26 COSMIC RO measurements. However, particular attention should be paid to EDP data below peak  
27 regions in application as data at bottom side of the profiles are less reliable than that at the peak and  
28 topside regions.

29 **Key words:** CSES satellite; COSMIC mission; radio occultation; validation; ionosphere

## 30 1. Introduction

31 The first China Seismo-Electromagnetic Satellite (CSES), also called ZH-1 in China, has been  
32 working for over 1 year since its launch on February 2, 2018. This satellite is the first spaced-based  
33 geophysical field measurement platform in China, which can be used for the 3-D earthquake  
34 observation when combining with the ground-based observation system; a subsequent satellite of  
35 this series will be launched in 2022 and the engineering work is under way. The primary scientific  
36 objectives of the CSES mission is to obtain world-wide data of space environment of the  
37 electromagnetic field, ionospheric plasma and charged particles, to monitor and study the  
38 ionospheric perturbations which may possibly associated with earthquake activity, especially with  
39 those destructive ones, to support the research on geophysics, space sciences as well as electric wave  
40 sciences and so on, and also to provide the data sharing service for international cooperation and  
41 scientific community (Shen et al., 2018).

1 The CSES satellite is sun synchronous orbit with an inclination angle of  $97.4^\circ$  at the altitude of  
2 507 km. The local time of descending and ascending nodes are 1400 and 0200 respectively. It takes  
3 about 94.6 minutes to complete a circular orbit, thus about 15 orbits per day. The revisiting period  
4 of CSES is 5 days, which means the satellite will nearly repeat the orbits after 5 days. At present,  
5 the observation range of the CSES satellite is mainly between  $-65^\circ$  and  $+65^\circ$  of geographic latitudes  
6 (Wang et al., 2019).

7 There are eight Chinese payloads and one Italian payload onboard the CSES satellite,  
8 belonging to 3 categories: (1) electromagnetic observations, including search-coil magnetometer  
9 (SCM), electric field detector (EFD), and high precision magnetometer (HPM); (2) ionosphere  
10 related observations, including GNSS occultation receiver (GOR), plasma analyzer package (PAP),  
11 Langmuir probe (LAP), and tri-band beacon (TBB); (3) and high-energy particles observations,  
12 including high energetic particle package (HEPP) and high energetic particle package detector  
13 (HEPD), of which HEPD is provided by Italian Space Agency.

14 Of the eight payloads, four are related to ionospheric parameter observations. The GOR  
15 payload onboard CSES is a GPS/BD2 receiver to retrieve ionospheric electron densities according  
16 to the radio wave refractivity when traversing the ionosphere. It is known that Low Earth Orbit  
17 (LEO) based GPS/GNSS radio occultation (RO) technique has been a powerful technique in  
18 ionosphere monitoring; using this technique, the accurate electron density profiles (EDPs) in the  
19 ionosphere can be derived with high vertical resolution on a global scale from bending information  
20 of the RO signals (Kuo et al., 2004; Rocken et al., 2000; Schreiner et al., 1999). Therefore, many  
21 LEO satellites were launched with RO payload after the pioneer RO experiment on GPS/MET  
22 mission (Hajj et al., 1998; Schreiner et al., 1999), such as the CHAMP satellite (Jakowski et al.,  
23 2002; Wickert et al., 2009), the GRACE satellites (Beyerle et al., 2005), the most famous COSMIC  
24 mission (Anthes et al., 2008; Lei et al., 2007), and so on. The application of RO technique is also  
25 an important part of the CSES satellite. Combining with the in situ electron density measurements  
26 onboard CSES, the CSES RO retrieved electron densities can be used to study global scale  
27 ionospheric 3D images from the bottom of the ionosphere to the altitude of the CSES satellite using  
28 the large amount of daily occultation events. However, a complete and thorough validation of the  
29 RO measurements obtained by the CSES satellite is a necessary work before the retrieved electron  
30 density profiles can be used for ionospheric studies.

31 A primary comparison, between CSES and COSMIC using the global distribution of peak  
32 values ( $N_mF_2$ ) and peak heights ( $h_mF_2$ ) data, was carried out during the in-orbiting test period of the  
33 CSES satellite, and the CSES  $N_mF_2$  values were also compared with the measurements from 3  
34 digisondes in China (Cheng et al., 2018). According to this paper, both the comparisons show that  
35 the CSES RO  $N_mF_2$  data are generally consistent with measurements from COSMIC and ionosondes.  
36 However, quantitative errors and application suggestions are not given in this paper. Moreover, the  
37 comparisons are limited to the peak values and the date coverage is only two months. Therefore, a  
38 more complete validation is still required to assess the consistency and reliability of the RO profiles  
39 obtained by the CSES satellite. A large amount of RO profiles have been obtained so far by CSES,  
40 which provide enough data to implement a more detailed validation work.

41 Validation of RO profiles is usually done by comparing the profiles with the measurements  
42 from ionospheric vertical sounding or incoherent scatter radars (ISRs). However, RO electron  
43 density profiles above the F2 peak region cannot be validated by ionosonde observations due to the  
44 unreliable extrapolating data at these altitudes. In addition, the uneven distribution of the ionosonde

1 stations, most located on continental areas and fewer in the ocean areas, restricts the global  
2 comparison work. Although ISRs can be used to validate RO electron density profiles above F2  
3 peak region, this comparison is limited due to the relatively small number of ISR sites as well as  
4 their limited operating time. Therefore, we will carry out the comparison work using the RO  
5 measurements from the COSMIC dataset in this paper.

6 Validation of the COSMIC electron density measurements has been performed in numerous  
7 studies using different measurements, such as the cross validation of the retrieved profiles from  
8 nearby spacecraft in the same COSMIC mission (Schreiner et al., 2007), comparison with ground-  
9 based ionosondes and ISRs (Cherniak and Zakharenkova, 2014; Chu et al., 2010; Chuo et al., 2011;  
10 Habarulema et al., 2014; Kelley et al., 2009; Krankowski et al., 2011; Lei et al., 2007; McNamara  
11 and Thompson, 2015), comparison with the in situ electron density measurements (Lai et al., 2013;  
12 Pedatella et al., 2015; Yue et al., 2011), comparison with radio tomography data using space  
13 climatology phenomenon (Thampi et al., 2011), comparison with ionospheric model IRI (Lei et al.,  
14 2007; Wu et al., 2015; Yang et al., 2009), and so on. As COSMIC RO data have been extensively  
15 validated and widely accepted for application, COSMIC RO data are used to validate the in situ  
16 plasma density observations from the Swarm constellation (Lomidze et al., 2017). We therefore also  
17 try to use the COSMIC RO dataset to validate CSES RO measurements because of its relative large  
18 amount of data with globally spatial coverage. In addition, similar RO retrieved data from the two  
19 sets also provides a unique opportunity to check the consistency and reliability of CSES  $N_mF_2$  and  
20  $h_mF_2$  parameters as well as RO profiles.

21 In this study, the validation work is implemented by comparing CSES  $N_mF_2$ ,  $h_mF_2$ , and data  
22 from EDPs at some selected altitudes with corresponding COSMIC measurements, and the bias and  
23 RMSE between the two sets are then calculated and estimated to evaluate the consistency and  
24 reliability of CSES RO retrieved data. Based on the results, an application suggestion is given on  
25 the CSES ionospheric RO data.

## 26 **2. Data and Method**

### 27 **2.1 CSES and COSMIC RO data**

#### 28 **1. CSES RO data**

29 GOR payload onboard CSES can receive the dual frequencies from GPS (L1:  
30 1575.42MHz±10MHz; L2: 1227.6MHz±10MHz) and DB2 (L1:1561.98MHz±2MHz; L2:  
31 1207.14MHz±2MHz) to retrieve atmospheric and ionospheric parameters with sampling rate of  
32 100Hz and 20Hz respectively. Firstly, TECs from GPS to LEO are calculated from the carrier phase  
33 of the dual frequencies; and then electron densities are retrieved from TECs using the Abel  
34 integration transformation. The Abel integration method and assumptions used in RO inversion  
35 process have been described in detail in many publications (Kuo et al., 2004; Lei et al., 2007;  
36 Schreiner et al., 1999) and will therefore not repeat here.

37 The GOR payload onboard CSES started to work on February 12, 2018 and ionospheric radio  
38 occultation (RO) measurements have been conducted since then. CSES RO retrieved data are  
39 divided into 5 levels: 0, 1, 2, 2A and 3. Level-0 is original data; Level-1 is physical quantity in time  
40 order; Level-2 is physical quantity data with satellite orbital information and geomagnetic

1 coordinates, while Level-2A is similar with Level 2, but with higher precise orbital information; and  
2 Level-3 is 2D structural data product from Level-2 and Level-2A, which can provide peak value,  
3 peak height and EDP data.

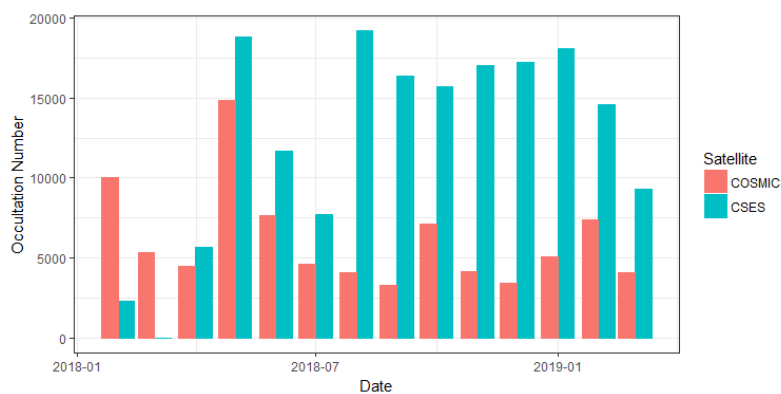
4 All the CSES RO data of the 5 levels are saved in HDF5 format, which is organized in a  
5 hierarchical way. One file is saved for each occultation event, and about 500 to 600 occultation event  
6 files can be obtained per day. Data users can refer to the data specification document for detailed  
7 description of data file naming conventions and data level classification, which can be obtained from  
8 the CSES data sharing center website [www.leos.ac.cn](http://www.leos.ac.cn).

9 More than 180,000 CSES occultation profiles have been obtained from 2018-02-12 to 2019-  
10 03-31, of which occultation events co-located with that from the COSMIC mission are used to carry  
11 out the comparison and validation work in this paper.

## 12 2. COSMIC RO data

13 The COSMIC (Constellation Observing System for Meteorology, Ionosphere, and Climate,  
14 also called FORMOSAT-3 in Taiwan) mission, a constellation of six identical low Earth orbit  
15 satellites launched in April 2006, is a joint Taiwan-US mission to observe the near-real-time GPS  
16 RO data (Anthes et al., 2008). COSMIC RO data come from the GPS Occultation Experiment (GOX)  
17 receivers onboard the COSMIC satellites that monitor the two GPS L-band signals to establish the  
18 relative geometries of satellite positions and differences in phase/Doppler shifts (Rocken et al.,  
19 2000). At the University Corporation for Atmospheric Research (UCAR) COSMIC Data Analysis  
20 and Archive Center (CDAAC), ionospheric profiles are retrieved by use of the Abel inversion  
21 technique from TEC along LEO-GPS rays. Detailed description of CDAAC data processing and  
22 EDP retrieval method can be found in some literatures (Kuo et al., 2004; Lei et al., 2007).

23 In the present study, the COSMIC level-2 electron density profiles provided as “ionPrf” files  
24 from 2018-02-12 to 2019-03-31 are used, which can be downloaded from CDAAC website  
25 <https://cdaa-www.cosmic.ucar.edu/>. COSMIC can provided over 2000-2500 RO profiles per day at  
26 its initial stage, but for now only 200-300 events on average can be obtained each day. Fig.1 gives  
27 the total occultation numbers of each month for both CSES and COSMIC missions from February  
28 2018 to March 2019.



29 Fig. 1 Occultation number per month from February 2018 to March 2019 for both CSES and COSMIC  
30 From Fig. 1 it can be seen that over 15,000 occultation events can be obtained by CSES each  
31 month, or over 500 per day on average, after the initial in-orbit testing stage from February 2018 to  
32 July 2018. In contrast, occultation numbers from COSMIC are much less, there are only about 200  
33 occultations on average each day. A total of over 86,000 occultation events have been obtained from  
34 the COSMIC data center from February 2018 to March 2019.  
35

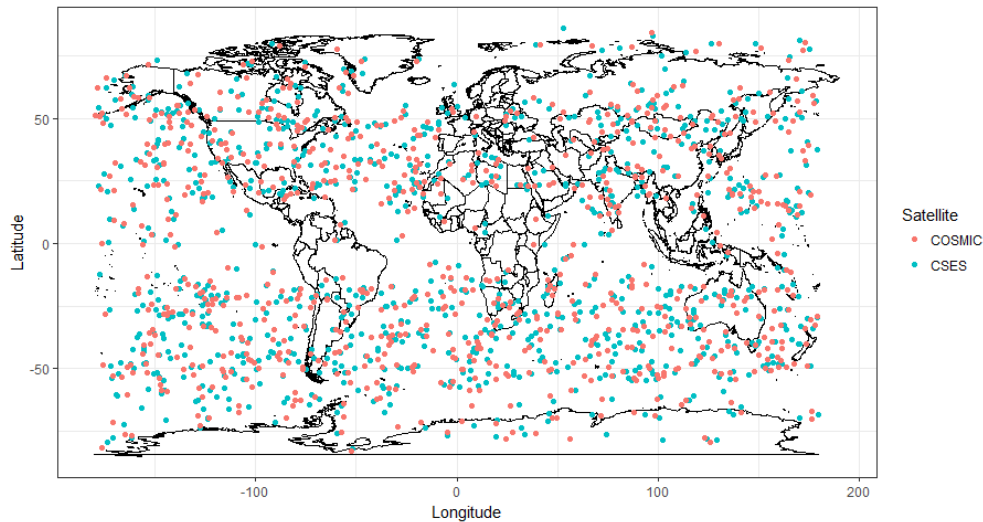
1 Based on these two datasets from CSES and COSMIC, the co-located occultations within  
2 defined spatial and temporal criteria from the two measurements are selected and used to carry out  
3 the comparison work.

## 4 **2.2 Data selection**

5 In order to make the comparison between CSES and COSMIC RO data as accurate as possible,  
6 spatial and temporal criteria must be defined to select matching occultation profiles for subsequent  
7 comparison analysis.

8 Before determining the selection criteria, it should be pointed out here that RO retrieved  
9 electron density profiles are different from those obtained by [vertical ISR observations](#). For the later,  
10 the observation point is fixed, and all the data points of different altitudes on the profiles correspond  
11 to this fixed observation point; but for the former, both the LEO and GPS are in motion during the  
12 occultation process, therefore data points of different altitudes on the profile correspond to different  
13 point on the ground. The geographic location of the tangent points of a RO retrieved profile may  
14 vary in several hundred kilometers, which means the spatial range of a profile can cover several  
15 degrees in horizontal latitude and longitude range, and several hundred kilometers in vertical altitude  
16 range. However, the ionospheric spatial correlation can extent to a large area as suggested by some  
17 researches (Shim et al., 2008; Yue et al., 2007). According to Shim et al. (2008), the daytime  
18 meridional correlation lengths are approximately  $9^\circ$  and  $5^\circ$  at mid- and low-latitudes, and the  
19 nighttime values are about  $3^\circ$  and  $2^\circ$  at mid- and low latitudes, respectively; the zonal correlation  
20 lengths are  $23^\circ$  at mid-latitudes and  $15^\circ$  at low latitudes during the day, and are  $11^\circ$  at mid-latitudes  
21 and  $10^\circ$  at low latitudes during the night. Therefore, the matching profile pairs from the two missions  
22 must be within the correlation distances. Considering the relatively small number of occultation  
23 events from the COSMIC measurements, we define the search criteria for co-located occultation  
24 events as follows: (1) the time difference between the matching occultation pairs is less than 30 min;  
25 (2) the distance differences between the locations of the two occultation events are within  $2^\circ \times 6^\circ$   
26 range in latitudinal and longitudinal directions. Here, the tangent point at F2 peak value of an  
27 occultation profile is defined as the location of the occultation event. The reason to use the peak  
28 value tangent point as the occultation location is because the peak value is normally located at the  
29 middle of a profile for the CSES EDPs, and by this way the spatial differences of the corresponding  
30 points, especially the top and bottom points, between the matching profile pairs can be limited to  
31 the correlation distance range as many as possible.

32 Based on the above criteria, the RO profiles from CSES and COSMIC, covering the period  
33 from February 2018 to March 2019, are searched to select the co-located profile pairs. The profiles  
34 with  $N_mF_2$  appearing below 200km or above 500 km are discarded, and profiles with only ascending  
35 or descending part of a profile which cannot determine the peak values are also deleted from the  
36 CSES dataset. A total of 845 matched profiles are found, and their distributions are given in Fig. 2.  
37 Numbers of occultation in each 10 latitudinal region are also calculated and given in Fig.3.



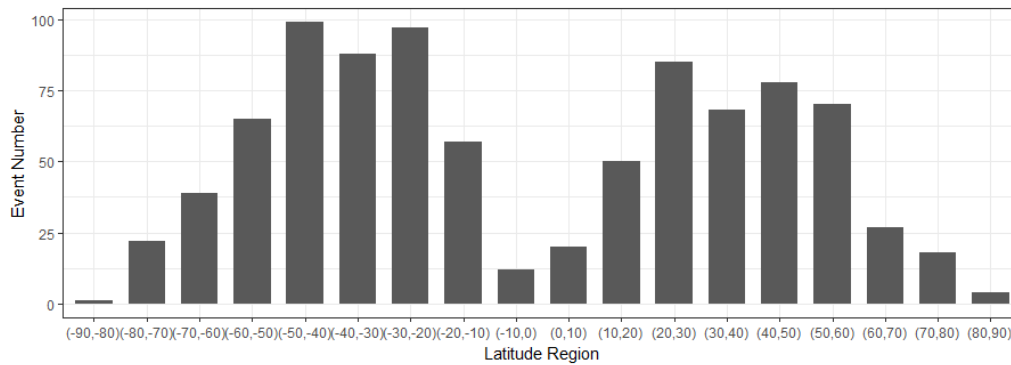
1

2

Fig. 2 Distribution of the selected profile pairs

3

(Each dot indicates the location of the tangent point of the maximum values in a profile.)



4

5

Fig. 3 Number of co-located profile pairs along latitudinal regions

6

From Fig.2, it can be seen that the selected profile pairs are globally distributed, which makes the data be representative of the whole dataset on spatial scale. In addition, the time coverage of the co-located occultation pairs is over a year, including different periodic components of the ionospheric variations, which makes the data involved in the comparison be representative on temporal scale also.

10

11

It is necessary to note that because the CSES satellite is sun-synchronous orbit as mentioned earlier, the local time of the occultation events is concentrated around the ascending (0200) and descending (1400) local time, while COSMIC data cover all the local time. Therefore, special attentions should be paid on the local time issue when combing CSES and COSMIC RO data together for data analysis, that is, occultation events with similar local time as that of CSES must be selected from the COSMIC dataset. This local time issue is not considered by Cheng et al. (2018) when they compared CSES RO data with that from COSMIC, therefore their result is questionable.

17

18

Another point to note is that most of the selected profile pairs are distributed in the mid-latitude regions, as shown in Fig. 2 and Fig. 3, and the equatorial region as well as the high latitude regions exhibit lower number of occultation events, which ensures that the selection criteria can be satisfied for most of the selected matched profiles.

21

## 1    **2.3 Comparison method**

2       The CSES RO electron density data are compared with the co-located COSMIC RO data to  
3 assess the consistency and reliability of the CSES RO data relative to that of the COSMIC, and then  
4 the consistency and reliability of the CSES RO data relative to ground-based measurements are  
5 estimated using the results obtained by previous researches on COSMIC RO data according to error  
6 propagation rules.

7       The maximum electron density and its height, namely  $N_mF_2$  and  $h_mF_2$  from CSES RO data, are  
8 compared and analyzed directly with the corresponding co-located COSMIC data, respectively.  
9 Besides RO peak values, the profiles of the matched pairs are also compared in this study. To  
10 compare the similarities of the profiles, average electron density data near some special altitudes of  
11 a profile are calculated and compared. Because the orbit altitude of CSES is 507km, only data below  
12 this altitude are obtained from the CSES RO retrieved EDPs. Therefore, some altitudes below this  
13 altitudes are selected, including 100, 150, 200, 250, 300, 350, 400, 450 and 500 km. It should be  
14 pointed out here that selection of these altitudes are of no particular meaning, but for simplification  
15 and ease of calculation. The consistency and reliability of the CSES RO profiles are thus evaluated  
16 by combining the comparison results of these selected altitudes.

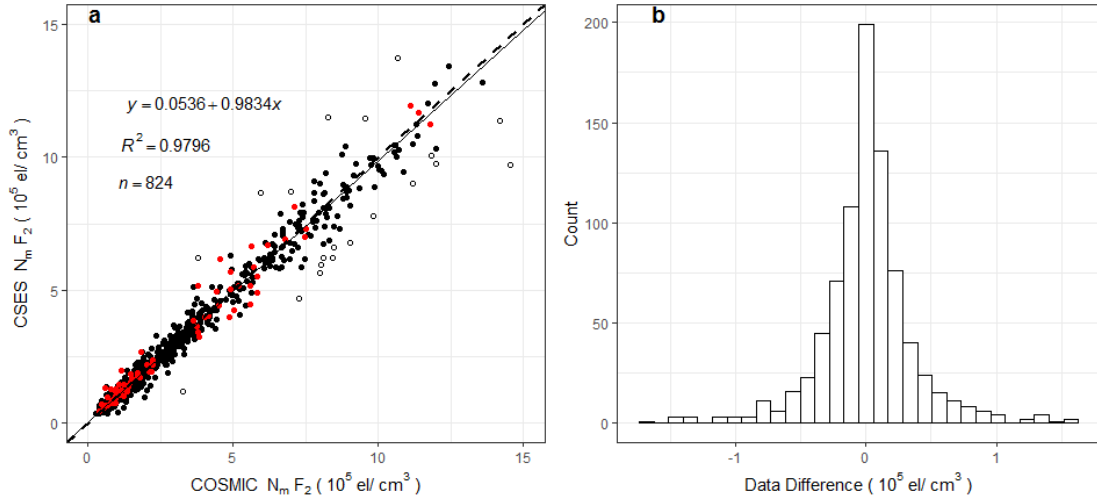
17       Normally, the height resolution in the F region has the order of 20 km for the COSMIC RO (Kuo  
18 et al., 2004), but CSES RO data has a higher resolution due to the higher sampling rate of the radio  
19 signals. We therefore use the average data between the selected altitudes  $\pm 10$ km, which is just within  
20 the vertical resolution of the COSMIC RO data.

21       In this study, all the selected matched profiles are involved in the analysis rather than those  
22 observed in geomagnetic quiet days. In this way, disturbed data caused by events such as  
23 geomagnetic storms can also be used to compare their similarities/differences under these special  
24 occasions.

## 25    **3. Results and Discussions**

### 26    **3.1 Comparison of $N_mF_2$**

27       The maximum electron density in the ionospheric F2 layer,  $N_mF_2$ , is the most important  
28 parameter in ionospheric related studies. To compare this parameter, the maximum electron density  
29 data are extracted from all the matched RO files of CSES and COSMIC measurements. Scatter plot  
30 of these matched  $N_mF_2$  points is given in Fig. 4, also given is the histogram of the data differences  
31 between the matched peak value points. As shown in Fig. 4b, data differences between the two  
32 measurements are normally distributed; points with data differences exceeding 3 times root mean  
33 square error (RMSE), shown as open circles in Fig. 4a, are considered outliers and can be eliminated  
34 from the selected dataset according to  $3\sigma$  rule. Red points in Fig. 4a are peak values observed during  
35 geomagnetic storm conditions of  $Dst < -30$  nT, all of which are within  $3\sigma$  limits and matched very  
36 well as shown in Fig. 4a. Fig. 4a also gives the linear fitting equation, the goodness-of-fit coefficient  
37  $R^2$  (square of correlation coefficient), and number of data points with elimination of outliers.



1

2

Fig. 4 Scatter plot of matched  $N_mF_2$ s and histogram of the data differences between the two sets

3

(The dash line in Fig. 4a is the equal value line with a slope of 1, and the solid line is the linear fitting line. Open circles are points exceeding 3 times RMSE. Red solid points are data observed when  $Dst < -30nT$ .  $y$  refers to CSES  $N_mF_2$  data,  $x$  COSMIC  $N_mF_2$  data.  $R^2$  is the goodness-of-fit coefficient;  $n$  is the total data number after eliminating outliers.)

4

5

6

7

The correlation coefficient between the two matched  $N_mF_2$  sets with elimination of outliers is 0.9898, and correlation coefficient without elimination of outliers is 0.9795, both of which can pass the significance test of confidence level 0.01. The high correlation coefficient indicates the high consistency between the two  $N_mF_2$  sets. The linear fitting coefficient of 0.9834 given in Fig. 4a is very close to 1; the data differences between the two sets are nearly normal distributed as shown in Fig. 4b, and most of the data differences is around zero, all of which mean that the CSES  $N_mF_2$ s are almost equal to COSMIC  $N_mF_2$ s with a nearly zero bias. Both the correlation coefficient and the linear fitting coefficient indicate that the CSES  $N_mF_2$ s are in extremely good agreement with the corresponding COSMIC data.

8

9

10

11

12

13

14

15

16

To quantify the error, we also calculate the RMSE and relative RMSE between the two sets. The mean of the data differences between CSES  $N_mF_2$  and COSMIC  $N_mF_2$  is  $0.005363 \times 10^5 / \text{cm}^3$ , and the RMSE between the two matched datasets is  $0.3638 \times 10^5 / \text{cm}^3$ , both of which are very small when comparing with the original data. Therefore, the nearly zero bias between the two measurements of  $N_mF_2$  can be neglected, which is in accord with the normal distribution with most data differences clustering around zero as shown in Fig. 4b. The mean relative differences or mean relative deviation (MRD) of  $N_mF_2$  is 1.97%, and the corresponding relative RMSE is 16.17%. The MRD is also extremely small. The mean of data differences and the mean of relative data differences, as well as their RMSEs, again show that the CSES RO data are in very good agreement with the COSMIC data.

17

18

19

20

21

22

23

24

25

26

To compare the difference of correlation relationship for daytime and nighttime data, the data in Fig. 4 are divided into two groups. As introduced in section 2.2, the local time of CSES satellite is fixed at 0200 during night and 1400 during day, and the local time of RO data are around these two fixed local time, we therefore don't need to further consider differences caused by different local time.

27

28

29

30

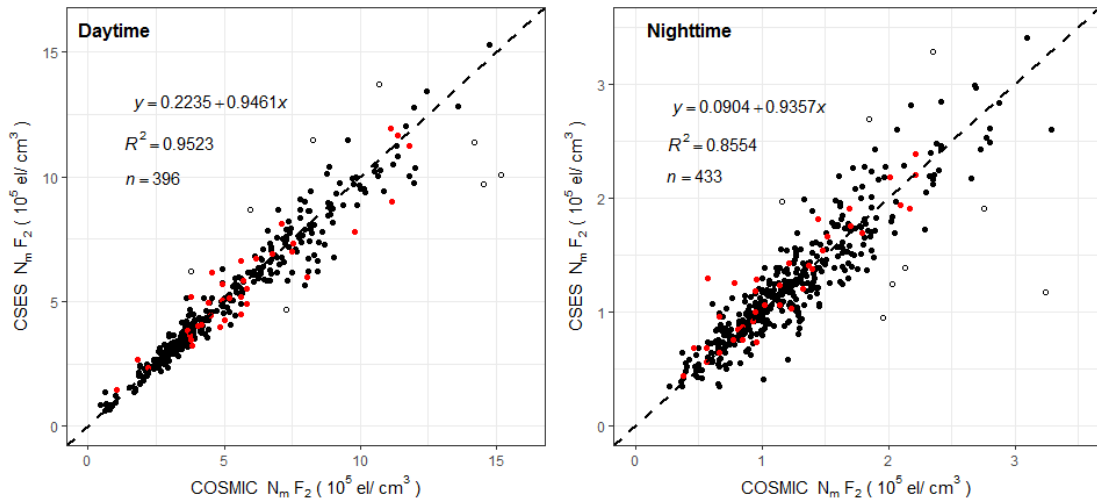
31

The scatter plots for daytime and nighttime data are drawn using the same method introduced above and given in Fig. 5. The data obtained under geomagnetic storm conditions are also shown in

32



1 red color, all of which are within the  $3\sigma$  limits.



2

3

Fig. 5 Scatter plot of  $N_mF_2$  for daytime and nighttime data

4

(the dash line in Fig. 5 is the equal value line with a slope of 1)

5

Correlation coefficient for daytime data with elimination of outliers is 0.9759, and 0.9628 without elimination of outliers; for nighttime data with elimination of outliers, correlation coefficient is 0.9249, and 0.8916 for all the data. The higher daytime correlation coefficient indicates a better agreement for the daytime data than the nighttime data. This can be seen clearly from Fig.5, the nighttime data are obviously fluctuated more violently.

10

The mean data differences for daytime data is  $-0.04346 \times 10^5 / \text{cm}^3$  with a RMSE of  $0.5865 \times 10^5 / \text{cm}^3$ , and mean data differences for nighttime data is  $0.01215 \times 10^5 / \text{cm}^3$  with a RMSE of  $0.1998 \times 10^5 / \text{cm}^3$ . The opposite sign of the daytime and nighttime mean data differences indicates that the CSES daytime data is slightly smaller than that of the COSMIC, while CSES nighttime data is slightly greater than the corresponding COSMIC data, but both the means of data differences are extremely small and can be consider zero bias when comparing with the original measurements.

16

Table 1 Absolute and relative error of  $N_mF_2$  between CSES and COSMIC

	Correlation coefficient	Absolute Error		Relative Error	
		Mean ( $/\text{cm}^3$ )	RMSE ( $/\text{cm}^3$ )	Mean	RMSE
Total	0.9898	$0.005363 \times 10^5$	$0.3638 \times 10^5$	1.97%	16.17%
Daytime	0.9759	$-0.04346 \times 10^5$	$0.5865 \times 10^5$	0.79%	12.76%
Nighttime	0.9249	$0.01215 \times 10^5$	$0.1998 \times 10^5$	2.61%	18.14%

17

(Results of all the coefficients and absolute errors maintain 4 significant digits, and relative errors maintain two digits after decimal point. Zeros are padded after the decimal point for some results to maintain an identical power exponent.)

20

When comparing the different results given in Table 1, the absolute mean data differences for daytime data is obviously greater than that of the overall result, and with an larger RMSE; and the mean data differences for nighttime data is also greater than the overall result, but with a smaller RMSE. It seems that nighttime data are in better agreement than daytime data. However, the two plots in Fig.5 indicate that the daytime data is obvious better than the nighttime data. This is because the daytime data are much greater than nighttime data, absolute error cannot correctly reflect the real situation when comparing data values with different magnitudes. We therefore calculate the relative errors for both the daytime and nighttime data. The mean relative data differences for

27

1 daytime data is 0.79% with a relative RMSE of 12.76%, and mean relative data difference for  
2 nighttime data 2.61% with a relative RMSE of 18.14%, which indicates an obvious better agreement  
3 for the daytime measurements.

4 It is necessary to point out that most of the daytime data points with higher values are located  
5 below the dash line as shown in Fig. 5, which means that the COSMIC  $N_mF_2$ s are larger than that  
6 of the CSES, so there is a negative bias between the two sets; while for nighttime data, most the data  
7 points with higher values are above the dash line, indicating greater CSES  $N_mF_2$  values, thus there  
8 is a positive bias between them. This can also explain why there is a higher correlation coefficient  
9 and a smaller mean data difference when combining daytime and nighttime data together.

10 Another issue should be pointed out here. As can be seen from Table 1, the absolute mean  
11 difference for daytime data is negative, while the mean relative differences is positive. Further  
12 analysis shows this different signs is caused by some points with much larger CSES  $N_mF_2$  values.

13 Here, we compare our results with previous studies and do some analysis.

14 Lei et al. (2007) obtained a correlation coefficient of 0.85 when comparing COSMIC  $N_mF_2$  with  
15 observations from 31 globally distributed SPIDR (The Space Physics Interactive Data Resource,  
16 <http://spidr.ngdc.noaa.gov/spidr>, which is no longer available) ionosondes using data observed in  
17 July 2006. Chuo et al. (2013) demonstrated that COSMIC derived  $N_mF_2$  values are in good  
18 agreement with digisonde observations of different seasons; they also reported an agreement about  
19 0.96 using observations from a lower latitude ionosonde in souther hemisphere using a big dataset  
20 from May 2006 to April 2008. Chu et al. (2010) found a correlation coefficient of 0.98 when  
21 comparing  $N_mF_2$ s between COSMIC and 60 globally distributed ionosondes belonging to SWPC  
22 (Space Weather Prediction Center), NOAA, using data from November 2006 to February 2007.  
23 Krankowski et al. (2011) obtained a very good correlation coefficient of 0.986 when validating  
24 COSMIC RO data in 2008 using measurements in European mid-latitude ionosondes. Our result of  
25 0.9898 is quite similar to, or even slightly better than those results, when considering the similar  
26 solar activity levels. A relative high correlation coefficient between CSES  $N_mF_2$  and ionosondes can  
27 be deduced since the correlation transitive conditions are satisfied according to Langford et al.  
28 (2001). We therefore obtained that CSES RO derived peak values are in very good agreement with  
29 COSMIC and ground-based measurements.

30 For  $N_mF_2$  relative errors, Krankowski et al. (2011) obtained a mean relative bias of 0.72% with  
31 a standard deviation of 8.42%, and the slope of the linear fitting line is 0.994 using a manual selected  
32 dataset in Europe, which is better than the results in this paper. Wu et al. (2009) got a -3.2% relative  
33 bias with a standard deviation of 20.7% when comparing  $N_mF_2$ s between COSMIC and 62 global  
34 ionosondes from SPIDR using data from July 2006 to Decemeber 2007. Yue et al. (2011, 2013)  
35 suggest that the ability to retrieve  $N_mF_2$  using the Abel inversion technique has an uncertainty about  
36 10%. Based on the linear fitting equation between CSES and COSMIC and on the  $N_mF_2$  relative  
37 errors between COSMIC and ground-based measurements, we can deduce that the relative errors  
38 between CSES peak values and ground-based measurements are comparable to prior results  
39 according to error propagation rules.

40 As to the absolute error, Kelley et al. (2009) obtained a RMSE of  $1.0 \times 10^5 / \text{cm}^3$  when comparing  
41 COSMIC data with ISR; Hajj et al. (2000) obtained a  $N_mF_2$  RMS difference of about  $1.5 \times 10^5 / \text{cm}^3$   
42 when comparing the GPS/MET measurements with nearby ionosonde data, and Jakowski et al.  
43 (2002) also obtained a similar RMS difference of about  $0.9 \times 10^5 / \text{cm}^3$  when comparing the CHAMP  
44 RO measurements to the in situ Langmuir probe data on the same satellite. Habarulema et al. (2014)

1 suggested that all RO data sets are close to the ionosonde data within similar error margin for both  
2 mid-latitude and low-latitude regions when comparing COSMIC, GRACE and CHAMP RO data  
3 with that of ionosondes. The absolute errors of our results are much smaller than these results,  
4 indicating an extremely good agreements between CSES and COSMIC RO  $N_mF_2$  and further  
5 confirming that CSES RO are also within the general error limit as proposed by Habarulema et al.  
6 (2014).

7 Better result of daytime data in this study is in accord with the conclusion obtained by Wu et al.  
8 (2009) and Yue et al. (2011). As we know, the nighttime data has a more complex spatial distribution  
9 pattern comparing to daytime data, because daytime data are affected by solar radiation, which  
10 makes the global distribution pattern of ionosphere simpler during day time. Larger inversion error  
11 will be produced when facing uneven spatial distribution of electron density due to the violence of  
12 spherical symmetry assumption of the Abel inversion method. The complex night time spatial  
13 distribution can also be proved by the smaller correlation distance during nighttime than that of  
14 daytime as discussed in section 3.2 (Shim et al., 2008).

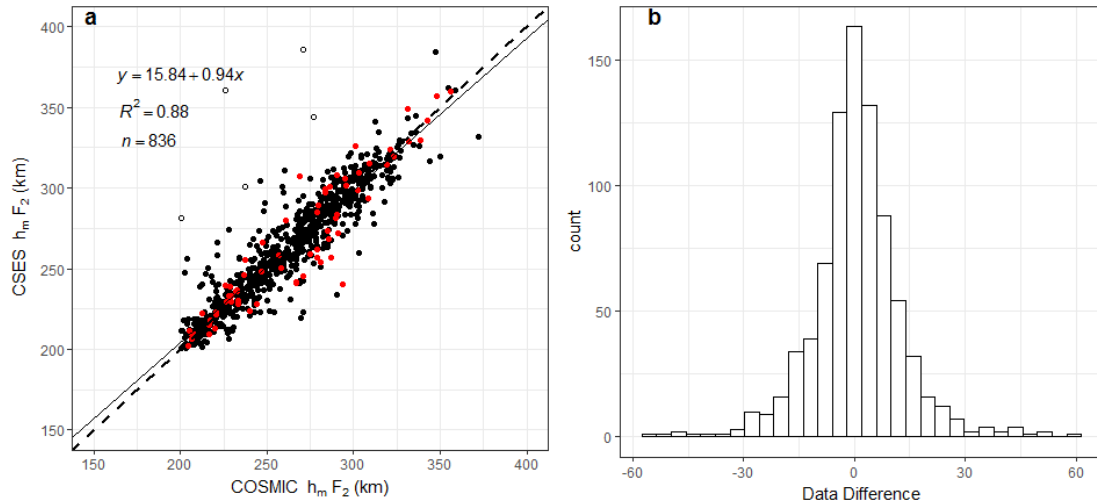
15 Besides data obtained under geomagnetic quiet days, data obtained under geomagnetic storm  
16 conditions are also quite consistent with each other, demonstrating that the RO data between CSES  
17 and COSMIC can remain consistency even under disadvantageous conditions. Hu et al. (2014)  
18 suggested that COSMIC measurements are acceptable under geomagnetic disturbed conditions  
19 when comparing COSMIC RO data with observations obtained from 2008 to 2013 at Sanya, a lower  
20 latitude ionosonde in China. We therefore deduce that CSES RO data may be acceptable under  
21 geomagnetic disturbed conditions, and we will validate this when enough RO data are accumulated.

22 As suggested by Schreiner et al. (2007) that co-located RO soundings allow the precision of the  
23 technique to be estimated, but not the accuracy. That fact that the nearly zero bias for both daytime  
24 and nighttime data and for the overall data, the normal distribution of the data differences, as well  
25 as the extremely high correlation coefficient between CSES  $N_mF_2$  and COSMIC  $N_mF_2$ , demonstrates  
26 that the CSES  $N_mF_2$  data are highly consistent and identical with COSMIC measurements, even  
27 under geomagnetic storm conditions, indicating a similar precision of CSES RO  $N_mF_2$  data as that  
28 of COSMIC. Given the reliability (accuracy) of the COSMIC data proved by many previous studies,  
29 we believe that the CSES  $N_mF_2$  measurements are also quite reliable. Since the co-located data  
30 points are globally distributed, the comparison results can be generalized to the overall CSES  $N_mF_2$   
31 dataset obtained so far.

### 32 **3.2 Comparison of $h_mF_2$**

33 The height of the maximum peak values in F2 layer,  $h_mF_2$ , is also a very important parameter  
34 for ionospheric studies. We therefore also compare this parameter using the corresponding COSMIC  
35 dataset.

36 Comparison of the  $h_mF_2$  values between the two sets using the same method as that by  $N_mF_2$ , the  
37 scatter plot of  $h_mF_2$  and the histogram of the data differences are given in Fig. 6. Data points  
38 exceeding 3 times of RMSE, shown as open circles in Fig. 6a, can be deleted from the selected data  
39 sets when calculation is implemented. Again, all the peak height points obtained under geomagnetic  
40 disturbed condition (red points) are within the  $3\sigma$  limits as shown in Fig. 6a. It can be seen clearly  
41 From Fig. 6a that most of the outliers (open circles) are obviously above the dash line, which means  
42 that occasionally RO data from the CSES dataset will much overestimate  $h_mF_2$  values.



1  
2  
3  
4  
5  
6  
7  
8  
9  
10  
11  
12  
13  
14  
15  
16  
17  
18  
19  
20  
21  
22  
23  
24  
25  
26  
27  
28  
29  
30

Fig. 6 Scatter plot of  $h_mF_2$ s for CSES and COSMIC and histogram of their differences

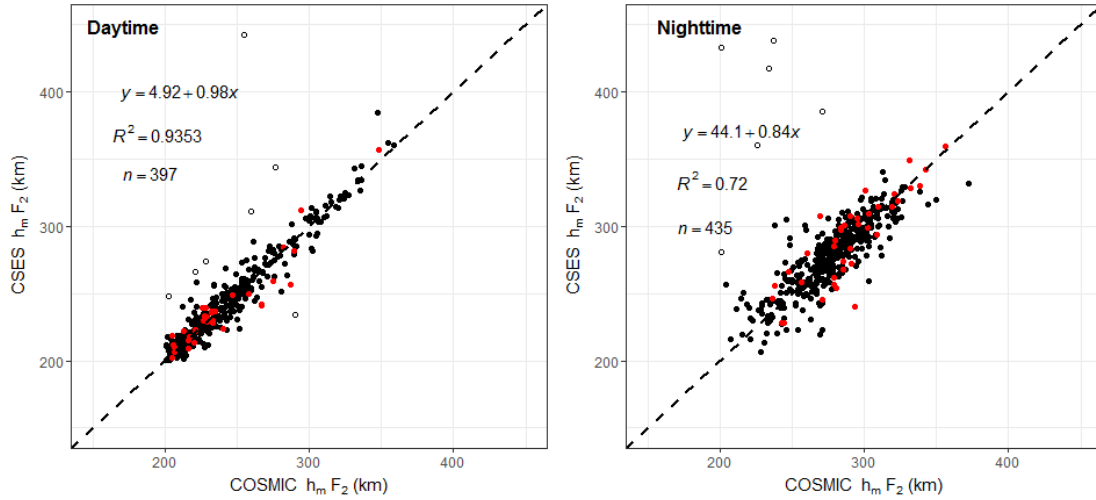
(The dash line is the equal values line with a slope of 1, and the solid line is the linear fitting line.  $y$  refers to the CSES  $h_mF_2$ , and  $x$  COSMIC  $h_mF_2$ . Open circles are points exceeding 3 times standard deviation of data differences between matched points. Red points are peak height obtained under geomagnetic condition of  $Dst < -30$  nT.)

The correlation coefficient of  $h_mF_2$  is 0.9385, though slightly lower than that of the  $N_mF_2$ , but can also pass the significance test of confidence level 0.01, which also indicates a very good agreement between the two sets of  $h_mF_2$ . The mean of the  $h_mF_2$  data differences (CSES  $h_mF_2$  minus COSMIC  $h_mF_2$ ) is 0.59 km, which indicates a slight greater  $h_mF_2$  for the CSES peak height values; and the RMSE is 12.28 km.  $h_mF_2$  data difference between the two sets is so small, which can be regarded as nearly zero bias.

Compared with  $N_mF_2$ ,  $h_mF_2$  data fluctuate more violently. It can be seen from Fig. 6a that some data points are obviously deviated from the data cluster, or from the equal value dash line. Data points above the dash line indicate that CSES  $h_mF_2$ s are greater than the corresponding COSMIC data, while data points below the dash line indicate a contrary situation that the COSMIC  $h_mF_2$ s are greater than that of CSES. Larger errors are produced by these obviously deviated situations. In spite of the data fluctuation, the nearly zero bias between the two sets, namely the mean data differences, are so small that it can be neglected, which is in accord with the nearly normal distribution of data differences as shown in Fig. 6b. The high correlation coefficient and the normally distributed data differences again indicate that the overall  $h_mF_2$  data of the two sets are in a good agreement.

We also compare the daytime and nighttime  $h_mF_2$ s and the corresponding scatter plots are given in Fig. 7. Correlation coefficient for daytime data is 0.9671, and for nighttime 0.8510. Similar as  $N_mF_2$ , daytime  $h_mF_2$  has a better correlation coefficient.

The mean data differences for daytime  $h_mF_2$ s is 0.40km with a RMSE of 8.59km; while the mean data differences for nighttime  $h_mF_2$ s is 0.62km with a RMSE of 14.30km. The positive means of data differences for both daytime and nighttime data indicate that the overall CSES  $h_mF_2$ s are slightly greater than that of the COSMIC, but they are so small and can be neglected. The greater RMSE of the nighttime data indicates an obvious more fluctuating nighttime  $h_mF_2$ s comparing to the daytime  $h_mF_2$ s.



1

2

Fig. 7 Scatter plot of  $h_mF_2$  for daytime and nighttime data

3

(the dash line in Fig. 5 is the equal values line with a slope of 1)

4

The bias and RMSE for overall, daytime and nighttime data are given in Table 2 for a comparison.

5

Table 2 Absolute error of  $h_mF_2$  between CSES and COSMIC

	Correlation coefficient	Mean (km)	RMSE (km)
Total	0.9385	0.59	12.28
Daytime	0.9671	0.40	8.59
Nighttime	0.8510	0.62	14.30

6

From the results shown in Table 2 and Table 1, it can be seen that correlation of  $N_mF_2$  is better than that of  $h_mF_2$  between the two sets. This result is in accord with the conclusion that the RO measurements were better in  $N_mF_2$  than in  $h_mF_2$  (Chuo et al., 2011). Another point is that the daytime  $h_mF_2$ s are in better agreement than the nighttime data, which is similar as that of  $N_mF_2$  data.

10

The overall comparison results of  $h_mF_2$  are very good when comparing to prior COSMIC RO data validation results using ionosondes observations. Chuo et al. (2013) reported an  $h_mF_2$  agreement about 0.87 using observations in low latitude southern hemisphere from May 2006 to April 2008. Krankowski et al. (2011) got a correlation coefficient of 0.949 when comparing COSMIC  $h_mF_2$  data observed in 2008 with that from ionosondes in European mid-latitudes. The high correlation coefficients of our result indicate that the two sets are in good agreement, and the high correlation coefficients between COSMIC  $h_mF_2$  and ionosondes from previous studies can further prove that CSES  $h_mF_2$ s are consistent with ionosonde observations based on correlation transitive rule mentioned in Section 3.1.

19

Krankowski et al. (2011) obtained a bias of 2.8km and a standard deviation of 11.5km when validating the COSMIC  $h_mF_2$  data. Cherniak and Zakharenkova (2014) showed that COSMIC  $h_mF_2$ s were in a good agreement with Kharkov ISR observations of different seasons in 2008-2009, and bias and standard deviations are less than 24 km and 29 km respectively. Habarulema et al. (2014) obtained an error limit about 30km when comparing COSMIC  $h_mF_2$ s with mid-latitude ionosonde using data in 2008. Yue et al. (2011) suggested that the retrieval uncertainty in  $h_mF_2$  is about 10km for COSMIC simulation analysis. The nearly zero bias and the small RMSE between  $h_mF_2$  of CSES and COSMIC demonstrate that F region peak height parameter obtained by CSES and COSMIC are extremely similar with each other, or in another way,  $h_mF_2$ s from the two sets have similar precision and accuracy. We therefore deduce that error between CSES  $h_mF_2$  and ground-based  $h_mF_2$  is

28

1 comparable to prior results according to error propagation rules.

2 As a result, the significant correlation coefficient and very small absolute RMSE in this study  
 3 indicate the consistent variations and similar precision of  $h_mF_2$  between CSES and COSMIC, and  
 4 the nearly zero bias indicates the two sets have similar accuracy. All of these results indicate that  
 5 CSES RO retrieved  $h_mF_2$ s are reliable considering the reliability of COSMIC RO data validated by  
 6 many previous studies.

### 7 3.3 Comparison of EDPs

8 Besides the two most important parameters  $N_mF_2$  and  $h_mF_2$ , electron density profiles (EDPs) are  
 9 also very important because EDPs can provide electron densities at different altitudes to depict  
 10 ionospheric 3D images from the bottom of ionosphere to the altitude of LEO satellite.

11 As EDPs from CSES and COSMIC have different altitudes due to the different satellite altitudes  
 12 of the two missions, only data under the altitude of the CSES satellite can be compared from the co-  
 13 located profiles. We therefore compare the retrieved EDP data at some selected altitudes as the  
 14 numbers of data points are not identical for each matched profile pairs, and altitudes of each  
 15 retrieved data are not identical for the two co-located profile pairs either.

16 For each altitude specified in section 2.3, we calculate the average data between altitude $\pm$ 10km  
 17 of each profile and then calculate the correlation coefficients using all the average data pairs at that  
 18 altitude. The results of all selected altitudes are given in Table 3. Fig.8 gives the scatter plots of all  
 19 these altitudes, and data obtained in geomagnetic disturbed condition are shown in red points, also  
 20 shown in the figure are the linear fitting equations, goodness-of-fit coefficients, and numbers of data  
 21 points involved in the calculation. Outliers are eliminated from the data sets using the same criteria  
 22 mentioned above.

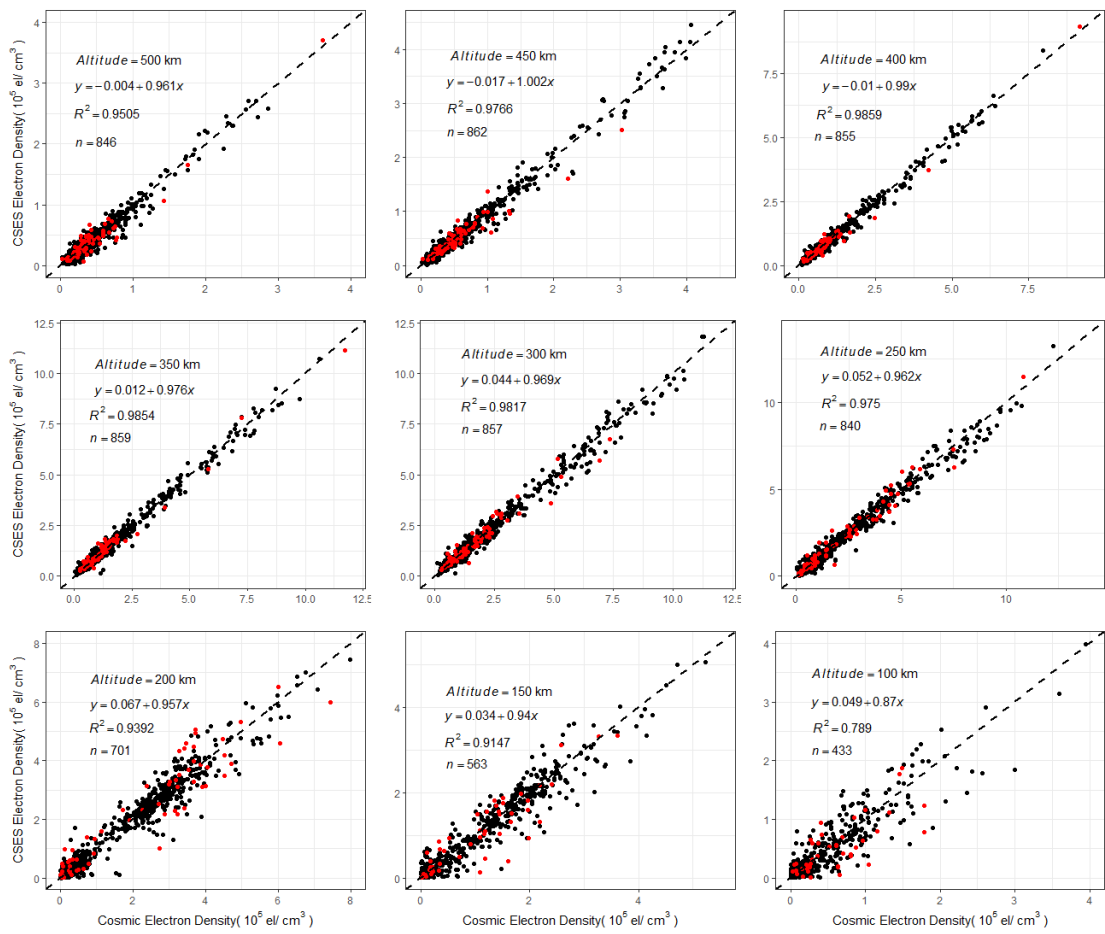
23 Table 3 Correlation coefficients and RMSEs for the data at different altitudes of the profiles

Altitude (km)	Correlation Coefficient	Absolute error		Relative error	
		Mean data difference	RMSE	Mean relative data differences	Relative RMSE
500	0.9749	-0.01982 $\times$ 10 <sup>5</sup>	0.8824 $\times$ 10 <sup>5</sup>	-1.72%	35.90%
450	0.9882	-0.01551 $\times$ 10 <sup>5</sup>	0.1070 $\times$ 10 <sup>5</sup>	-0.69%	27.30%
400	0.9929	-0.01923 $\times$ 10 <sup>5</sup>	0.1314 $\times$ 10 <sup>5</sup>	-0.59%	20.29%
350	0.9927	-0.02274 $\times$ 10 <sup>5</sup>	0.1946 $\times$ 10 <sup>5</sup>	0.74%	23.45%
300	0.9908	-0.01881 $\times$ 10 <sup>5</sup>	0.2700 $\times$ 10 <sup>5</sup>	1.89%	25.16%
250	0.9874	-0.03198 $\times$ 10 <sup>5</sup>	0.3309 $\times$ 10 <sup>5</sup>	4.70%	61.29%
200	0.9691	-0.01090 $\times$ 10 <sup>5</sup>	0.3909 $\times$ 10 <sup>5</sup>	25.83%	133.77%
150	0.9564	-0.03161 $\times$ 10 <sup>5</sup>	0.2958 $\times$ 10 <sup>5</sup>	43.28%	324.74%
100	0.8883	-0.02330 $\times$ 10 <sup>5</sup>	0.2611 $\times$ 10 <sup>5</sup>	78.40%	518.99%

24 All the correlation coefficients in Table 3 can pass the significance test of confidence level 0.01,  
 25 which means that data points at different altitudes are highly correlated. When combining all the  
 26 results together, we can deduce that the co-located profiles from CSES and COSMIC sets are quite  
 27 similar to each other in spite of the global distribution of these profile pairs as shown in Fig. 2 in  
 28 Section 2.2. According to some studies, COSMIC profiles are in very good agreement with  
 29 observations from different ISRs (Lei et al., 2007; Kelley et al., 2009; Cherniak and Zakharenkova,  
 30 2014). Pedatella et al. (2015) compared COSMIC RO data at different altitudes with in situ

1 observations from CHAMP and C/NOSF and obtained the correlation coefficients are greater than  
 2 0.90, proving the consistency of the COSMIC profiles with in situ satellite observations. Based on  
 3 the high consistency between CSES and COSMIC profile pairs and previous COSMIC EDP  
 4 validation results, we can deduce that CSES profiles may generally agree with ISR profiles  
 5 according to similarity transitive rules mentioned earlier (Langford et al., 2011), which we will  
 6 further prove by using ISR observations in our subsequent work.

7 Schreiner et al. (2007) showed that RMS is about  $10^3/\text{cm}^3$  between 150 to 500km altitude,  
 8 whereas below 150km the RMS increases to a maximum of about  $3 \times 10^3/\text{cm}^3$  at about 100km, when  
 9 comparing the RO profiles from different COSMIC satellites within 5km distance. Comparing  
 10 COSMIC profiles with ISR observations, Lei et al. (2007) suggested inversed errors are larger than  
 11  $10^5/\text{cm}^3$  at altitudes below  $\sim 150\text{km}$  and Cherniak and Zakharenkova (2014) obtained an error range  
 12 of  $12\text{-}16 \times 10^4/\text{cm}^3$ . Pedatella et al. (2015) obtained an overall bias of  $0.22 \times 10^5/\text{cm}^3$  with a standard  
 13 deviation of  $0.65 \times 10^5/\text{cm}^3$ , and relative bias and standard deviation are 14.9% and 10.4%  
 14 respectively, when validating COSMIC data at different altitudes using CHAMP in situ observations;  
 15 they also compared COSMIC data with C/NOFS in situ observations, and got a relative bias of 5.6%  
 16 with a standard deviation 12.4%. They attributed the better agreement with in situ observations from  
 17 C/NOFS to the higher altitude of this satellite. Both the absolute and relative errors, as well as error  
 18 variation with altitudes shown in Table 3, are in accord with those studies, suggesting that the CSES  
 19 EDPs are reliable and within general error limits due to the high similarity and consistency between  
 20 CSES and COSMIC EDPs.



21  
 22

Fig. 8 Scatter plots of data from matched profiles at different altitudes

1 (the dash line in Fig. 5 is the equal values line with a slope of 1)

2 From the correlation coefficients given in Table 3, it can be seen that correlation coefficients  
3 above 200 km are obviously greater than those below this altitude. The absolute mean differences  
4 at different altitudes are comparable to each other. However, relative differences at different altitudes  
5 are quite different; relative mean differences above 200km are extremely small, while relative mean  
6 differences below this altitude (include this altitude) increase dramatically. We obtained from Fig. 5  
7 that the peak heights  $h_m F_2$  of most profiles are located between 200km to 350km, the obviously high  
8 correlation coefficients in these regions indicate that RO retrieved data at and above peak height are  
9 more consistent with each other, whereas discrepancies between the two data sets below the peak  
10 regions are much larger. This can be explained by the distribution characteristics of the different  
11 ionospheric layers, and by the spherical assumption used in Abel inversion method. As we know,  
12 electron density fluctuations in regions above the F2 peak become smaller under geomagnetic quiet  
13 condition if comparing with that at lower altitudes due to the relative lower density according to  
14 electron density attenuation rules, it is therefore easier to satisfy the spherical symmetry assumption  
15 when using the Abel inversion method in this region. This spherical symmetry assumption is by far  
16 the most significant error source in the retrieval of the electron density profiles (Lei et al., 2007). In  
17 addition, a shorter propagating distance in the topside ionosphere for the radio signals from GPS to  
18 LEO will lead to a smaller error of straight line propagation assumption. As suggested by Liu et al.  
19 (2010) that COSMIC RO can obtain reasonable correct electron densities around and above F2 peak;  
20 however, assumption of spherical symmetry introduces artificial plasma cave and plasma tunnel  
21 structures as well as electron density enhancement at the geomagnetic equator at and below 250 km  
22 altitude, which will enlarge data discrepancies as shown in Table 3. Syndergaard et al. (2006) also  
23 suggested larger errors at the bottom of the retrieved profiles. The results shown in Table 3 in this  
24 study are in accord with those studies, demonstrating that CSES EDPs have larger errors for data  
25 below 200km altitude, which is similar as that of COSMIC.

26 An obvious characteristic shown in Table 3 is that all the means of data difference are negative  
27 values though they are very small compare to the original measurements, which means the overall  
28 CSES data at different altitudes are smaller than the corresponding COSMIC data. The all negative  
29 mean data differences at different altitudes may indicate a possible systematic bias between the two  
30 measurements. This systematic lower values at all altitudes is most likely caused by the first-order  
31 estimation of the electron density at the altitude of the CSES satellite, rather than the spatial  
32 differences of the co-located profile pairs, because spatial differences lead to random errors.  
33 However, further confirmation of this error sources is required. It is also necessary to point out that  
34 the signs of the mean relative data differences at altitudes  $\geq 400$ km are negative, similar as the signs  
35 of the corresponding absolute errors; whereas the signs of the mean relative data differences at  
36 altitudes below 400km are positive, just on the contrary to the signs of absolute mean data  
37 differences. Further analysis shows that the opposite signs are caused by points where CSES data  
38 are much larger than that of COSMIC, and thus lead to extremely larger relative errors, which further  
39 indicates that data below the peak regions, especially below about 150km, fluctuate more violently.

40 Besides spherical symmetry and straight line propagation assumptions, the larger discrepancies  
41 at altitudes below peak regions can be explained by the different spatial locations of the matched  
42 profiles. Although the peak values of co-located profile pairs are near each other according to  
43 selection criteria, data points other than peak values on the matched profile pairs may exceed the  
44 selection criteria and result in larger distances due to the different tangent point path of the matched



1 profile pairs. As a result, a larger distance will lead to larger discrepancy between the corresponding  
2 data sets. In addition, the tangent point path of the matched profiles may have different directions,  
3 which will lead to different inversion results because each retrieved data represents average electron  
4 densities along the radio ray path. In regions with large horizontal gradients, the different ray path  
5 can cause obvious difference between the matched profiles. At altitudes below 200km, especially  
6 below 150 km, sporadic E-layers can cause large horizontal gradients, and then lead to large  
7 inversion error. Wu et al. (2009) suggested that the large relative error below 150 km is due to the  
8 errors transferred from upper altitude (the F layer) and the very small electron density at that altitude.  
9 They also suggested that the larger ray separations can induce larger errors which can be transferred  
10 to low altitudes; phase measurement errors induce small relative fluctuations on the electron density  
11 at the topside ionosphere, but can cause large relative fluctuations at low altitude ionosphere,  
12 because small electron density at low altitude is sensitive to the phase errors. It is therefore  
13 concluded that many sources can cause large errors for measurements at altitudes below 150km,  
14 which as a result lead to the large discrepancies between CSES and COSMIC RO data at the bottom  
15 of the ionosphere.

16 Based on the above analysis, we conclude that CSES RO profiles are generally consistent with  
17 that of COSMIC very well and are reliable for data applications due to the wide acceptance and  
18 application of COSMIC RO data. However, larger discrepancies are found at lower altitudes  
19 between the two sets comparing to data differences at higher altitudes. Therefore, special attention  
20 should be paid to data below 200km in applications due to the relative large discrepancies between  
21 the two datasets.

#### 22 **4. Summary and Conclusions**

23 Validation of the CSES RO data is carried out to estimate the consistency and reliability of the  
24 CSES RO data using the globally distributed measurements from the COSMIC mission covering  
25 the date range from February 12, 2018 to March 31, 2019 as COSMIC RO data have been widely  
26 validated their consistency and reliability using data from different measurements in global scale.  
27 Comparing CSES  $N_mF_2$ ,  $h_mF_2$ , and EDP data at some selected altitudes, with corresponding  
28 COSMIC RO data, we obtain the following results.

- 29 (1) CSES  $N_mF_2$  data are highly consistent with that from COSMIC with a correlation coefficient of  
30 0.9898. The mean data differences is  $0.005363 \times 10^5 / \text{cm}^3$  with a RMSE of  $0.3638 \times 10^5 / \text{cm}^3$ ; the  
31 relative mean differences is 1.970% with a relative RMSE of 16.17%. Correlation between  
32 daytime  $N_mF_2$  data is obviously better than that of nighttime  $N_mF_2$  data.
- 33 (2) CSES  $h_mF_2$  data are also very consistent with COSMIC data, with a correlation coefficient of  
34 0.9385. The bias between the two sets is 0.59km with a RMSE of 12.28km. Again, daytime  
35  $h_mF_2$  has a better correlation than nighttime data.
- 36 (3) Co-located profiles between CSES and COSMIC are generally consistent with each other very  
37 well, with a better agreement for data at and above peak height regions (200km) than those  
38 below this regions. For EDP data below 200km altitude, special attention should be paid due to  
39 the relative larger discrepancies between the two sets.
- 40 (4) Based on the validation results between COSMIC data and different measurements obtained by  
41 many previous studies and the validation results between COSMIC and CSES RO data obtained  
42 in this study, it is deduced that CSES RO data are within the error limits obtained by previous

1 studies according to error propagation rules.

2 GOX payload onboard CSES satellite can obtain over 500 occultation events each day, which  
3 provide a large dataset for the study of 3D distribution of the ionospheric electron density when  
4 combining with the in situ electron density measurements obtained by LAP onboard CSES. The  
5 relatively thorough comparison work in this paper demonstrates that the CSES RO data are  
6 consistent very well with the corresponding COSMIC data, proving that the CSES RO data are  
7 reliable for applications on ionospheric-related problems considering the wide applications of the  
8 COSMIC RO data. However, as many RO related studies suggest that asymmetry of electron density  
9 distribution is the main source of the Abel inversion transformation (Schreiner et al., 1999;  
10 Syndergaard et al., 2006; Lei et al., 2007), and this inversion error varies with solar activity, season,  
11 geomagnetic latitude and local time (Wu et al., 2009). The CSES RO data in this study cover all the  
12 latitudes and four seasons with fixed local time under lower solar activity condition, and solar  
13 activity in this study is similar as most of the COSMIC validation studies, the comparison results  
14 will therefore applicable to data with similar low solar activity conditions. More subsequent  
15 validation work will be conducted and presented using data accumulated under different solar  
16 activities.

## 17 **Author contribution**

18 Xiuying Wang arranged this study, including: experiment design and data analysis.

19 Wanli Cheng and Zihan Zhou collected the COSMIC data used in this paper.

20 Song Xu, Dehe Yang, and Jing Cui did some calculation work to search co-located data.

## 21 **Competing interests**

22 All authors declare that they have no competing interests.

## 23 **Acknowledgement**

24 This work is supported by the National Key R&D Program of China under Grant no.  
25 2018YFC1503505, by the Foundation of Institute of Crustal Dynamics, CEA under grant no.  
26 ZDJ2018-18 and ZDJ2019-03. COSMIC Radio Occultation data can be downloaded from  
27 <https://cdaac-www.cosmic.ucar.edu/> (last access: 22 August, 2019).

## 28 **Reference**

29 Anthes, R. A., Bernhardt, P. A., Chen, Y., Cucurull, L., Dymond, K. F., Ector, D., et al.: The COSMIC/FORMOSAT-3 Mission: Early  
30 Results, *Bulletin of the American Meteorological Society*, 89(3), 313–334, doi:10.1175/bams-89-3-313, 2008.

31 Beyerle, G.: GPS radio occultation with GRACE: Atmospheric profiling utilizing the zero difference technique, *Geophysical*  
32 *Research Letters*, 32, L13806, doi:10.1029/2005gl023109, 2005.

33 Cheng Y., Lin J., Shen X. H., Wan X., Li X. X., and Wang W. J.: Analysis of GNSS radio occultation data from satellite ZH-01, *Earth*  
34 *and Planetary Physics*, 2(6), 499-504, <https://doi.org/10.26464/epp2018048>, 2018.

35 Cherniak, I. V., and Zakharenkova, I. E.: Validation of FORMOSAT-3/COSMIC radio occultation electron density profiles by  
36 incoherent scatter radar data, *Advances in Space Research*, 53(9), 1304–1312, doi:10.1016/j.asr.2014.02.010, 2014.

37 Chu, Y.-H., Su, C.-L., and Ko, H.-T.: A global survey of COSMIC ionospheric peak electron density and its height: A comparison

1 with ground-based ionosonde measurements, *Advances in Space Research*, 46(4), 431–439, doi:10.1016/j.asr.2009.10.014,  
2 2010.

3 Chuo, Y.-J., Lee, C.-C., Chen, W.-S., and Reinisch, B. W.: Comparison between bottomside ionospheric profile parameters  
4 retrieved from FORMOSAT3 measurements and ground-based observations collected at Jicamarca, *Journal of Atmospheric and*  
5 *Solar-Terrestrial Physics*, 73(13), 1665–1673, doi:10.1016/j.jastp.2011.02.021, 2011.

6 Chuo, Y. J., Lee, C. C., Chen, W. S., and Reinisch, B. W.: Comparison of the characteristics of ionospheric parameters obtained  
7 from FORMOSAT-3 and digisonde over Ascension Island, *Annales Geophysicae*, 31(5), 787–794, doi:10.5194/angeo-31-787-2013,  
8 2013.

9 Habarulema, J. B., Katamzi, Z. T., and Yizengaw, E.: A simultaneous study of ionospheric parameters derived from FORMOSAT-  
10 3/COSMIC, GRACE, and CHAMP missions over middle, low, and equatorial latitudes: Comparison with ionosonde data, *Journal of*  
11 *Geophysical Research: Space Physics*, 119(9), 7732–7744, doi:10.1002/2014ja020192, 2014.

12 Hajj, G. A., and Romans, L. J.: Ionospheric electron density profiles obtained with the Global Positioning System: Results from  
13 the GPS/MET experiment, *Radio Science*, 33(1), 175–190, doi:10.1029/97rs03183, 1998.

14 Hu, L., Ning, B., Liu, L., Zhao, B., Chen, Y., and Li, G.: Comparison between ionospheric peak parameters retrieved from COSMIC  
15 measurement and ionosonde observation over Sanya, *Advances in Space Research*, 54(6), 929–938,  
16 doi:10.1016/j.asr.2014.05.012, 2014.

17 Jakowski, N., Wehrenpfennig, A., Heise, S., Reigber, C., Lühr, H., Grunwaldt, L., and Meehan, T. K.: GPS radio occultation  
18 measurements of the ionosphere from CHAMP: Early results, *Geophysical Research Letters*, 29(10), 95–1–95-4,  
19 doi:10.1029/2001gl014364, 2002.

20 Kelley, M. C., Wong, V. K., Aponte, N., Coker, C., Mannucci, A. J., and Komjathy, A.: Comparison of COSMIC occultation-based  
21 electron density profiles and TIP observations with Arecibo incoherent scatter radar data, *Radio Science*, 44, RS4011,  
22 doi:10.1029/2008rs004087, 2009.

23 Krankowski, A., Zakharenkova, I., Krypiak-Gregorczyk, A., Shagimuratov, I. I., and Wielgosz, P.: Ionospheric electron density  
24 observed by FORMOSAT-3/COSMIC over the European region and validated by ionosonde data, *Journal of Geodesy*, 85(12), 949–  
25 964, doi:10.1007/s00190-011-0481-z, 2011.

26 Kuo, Y.-H., Wee, T.-K., Sokolovskiy, S., Rocken, C., Schreiner, W., Hunt, D., and Anthes, R.: Inversion and Error Estimation of GPS  
27 Radio Occultation Data, *Journal of the Meteorological Society of Japan*, 82(1B), 507–531, doi:10.2151/jmsj.2004.507, 2004.

28 Lai, P.-C., Burke, W. J., and Gentile, L. C.: Topside electron density profiles observed at low latitudes by COSMIC and compared  
29 with in situ ion densities measured by C/NOFS, *Journal of Geophysical Research: Space Physics*, 118(5), 2670–2680,  
30 doi:10.1002/jgra.50287, 2013.

31 Langford, E., Schwertman, N., and Owens, M.: Is the Property of Being Positively Correlated Transitive? *The American*  
32 *Statistician*, 55(4), 322–325, doi:10.1198/000313001753272286, 2001.

33 Lei, J., Syndergaard, S., Burns, A. G., Solomon, S. C., Wang, W., Zeng, Z., et al.: Comparison of COSMIC ionospheric  
34 measurements with ground-based observations and model predictions: Preliminary results, *Journal of Geophysical Research:*  
35 *Space Physics*, 112, A07308, doi:10.1029/2006ja012240, 2007.

36 Liu, J. Y., Lin, C. Y., Lin, C. H., Tsai, H. F., Solomon, S. C., Sun, Y. Y., et al.: Artificial plasma cave in the low-latitude ionosphere  
37 results from the radio occultation inversion of the FORMOSAT-3/COSMIC, *Journal of Geophysical Research: Space Physics*, 115,  
38 A07319, doi:10.1029/2009ja015079, 2010.

39 Lomidze, L., Knudsen, D. J., Burchill, J., Kouznetsov, A., and Buchert, S. C.: Calibration and Validation of Swarm Plasma Densities  
40 and Electron Temperatures Using Ground-Based Radars and Satellite Radio Occultation Measurements. *Radio Science*, 53(1), 15–  
41 36, doi:10.1002/2017rs006415, 2018.

42 McNamara, L. F., and Thompson, D. C.: Validation of COSMIC values of foF2 and M(3000)F2 using ground-based ionosondes.  
43 *Advances in Space Research*, 55(1), 163–169, doi:10.1016/j.asr.2014.07.015, 2015.

44 Pedatella, N. M., Yue, X., and Schreiner, W. S.: Comparison between GPS radio occultation electron densities and in situ satellite

1 observations, *Radio Science*, 50(6), 518–525, doi:10.1002/2015rs005677, 2015.

2     Rocken, C., Kuo, Y.-H., Schreiner, W., Hunt, D., Sokolovskiy, S., and McCormick, C.: COSMIC system description, *Terr. Atmos.*  
3 *Ocean Sci.*, 11(1), 21–52, DOI: 10.3319/TAO.2000.11.1.21(COSMIC), 2000.

4     Schreiner, W., Rocken, C., Sokolovskiy, S., Syndergaard, S., and Hunt, D.: Estimates of the precision of GPS radio occultations  
5 from the COSMIC/FORMOSAT-3 mission, *Geophysical Research Letters*, 34, L04808, doi:10.1029/2006gl027557, 2007.

6     Schreiner, W. S., Sokolovskiy, S. V., Rocken, C., and Hunt, D. C.: Analysis and validation of GPS/MET radio occultation data in  
7 the ionosphere, *Radio Science*, 34(4), 949–966, doi:10.1029/1999rs900034, 1999.

8     Shen, X., Zhang, X., Yuan, S., Wang, L., Cao, J., Huang, J., et al.: The state-of-the-art of the China Seismo-Electromagnetic  
9 Satellite mission, *Science China Technological Sciences*, 61(5), 634–642, doi:10.1007/s11431-018-9242-0, 2018.

10     Shim, J. S., Scherliess, L., Schunk, R. W., and Thompson, D. C.: Spatial correlations of day-to-day ionospheric total electron  
11 content variability obtained from ground-based GPS, *Journal of Geophysical Research: Space Physics*, 113, A09309,  
12 doi:10.1029/2007ja012635, 2008.

13     Syndergaard, S., W. S. Schreiner, C. Rocken, D. C. Hunt, and K. F. Dymond: Preparing for COSMIC: Inversion and analysis of  
14 ionospheric data products, in *Atmosphere and Climate: Studies by Occultation Methods*, edited by U. Foelsche, G. Kirchengast,  
15 and A. K. Steiner, pp. 137–146, Springer, New York, 2006.

16     Thampi, S. V., Yamamoto, M., Lin, C., and Liu, H.: Comparison of FORMOSAT-3/COSMIC radio occultation measurements with  
17 radio tomography, *Radio Science*, 46, RS3001, doi:10.1029/2010rs004431, 2011.

18     Wang, X., Cheng, W., Yang, D., and Liu, D. Preliminary validation of in situ electron density measurements onboard CSES using  
19 observations from Swarm Satellites, *Advances in Space Research*, doi:10.1016/j.asr.2019.05.025, 2019.

20     Wickert, J., Michalak, G., Schmidt, T., Beyerle, G., Cheng, C.-Z., Healy, S. B.: GPS Radio Occultation: Results from CHAMP, GRACE  
21 and FORMOSAT-3/COSMIC, *Terrestrial, Atmospheric and Oceanic Sciences*, 20(1), 35-50, doi:10.3319/tao.2007.12.26.01(f3c),  
22 2009.

23     Wu, X., Hu, X., Gong, X., Zhang, X., and Wang, X.: Analysis of inversion errors of ionospheric radio occultation, *GPS Solutions*,  
24 13(3), 231–239, doi:10.1007/s10291-008-0116-x, 2009.

25     Wu, K.-H., Su, C.-L., and Chu, Y.-H.: Improvement of GPS radio occultation retrieval error of E region electron density: COSMIC  
26 measurement and IRI model simulation, *Journal of Geophysical Research: Space Physics*, 120(3), 2299–2315,  
27 doi:10.1002/2014ja020622, 2015.

28     Yang, K.-F., Chu, Y.-H., Su, C.-L., Ko, H.-T., and Wang, C.-Y.: An Examination of FORMOSAT-3/COSMIC Ionospheric Electron  
29 Density Profile: Data Quality Criteria and Comparisons with the IRI Model, *Terrestrial, Atmospheric and Oceanic Sciences*, 20(1),  
30 193-206, doi:10.3319/tao.2007.10.05.01(f3c), 2009.

31     Yue, X., Schreiner, W. S., Kuo, Y.-H., Wu, Q., Deng, Y., and Wang, W.: GNSS radio occultation (RO) derived electron density  
32 quality in high latitude and polar region: NCAR-TIEGCM simulation and real data evaluation, *Journal of Atmospheric and Solar-*  
33 *Terrestrial Physics*, 98, 39–49, doi:10.1016/j.jastp.2013.03.009, 2013.

34     Yue, X., Schreiner, W. S., Rocken, C., and Kuo, Y.-H.: Evaluation of the orbit altitude electron density estimation and its effect  
35 on the Abel inversion from radio occultation measurements, *Radio Science*, 46, RS1013, doi:10.1029/2010rs004514, 2011.

36     Yue, X., Wan, W., Liu, L., and Mao, T.: Statistical analysis on spatial correlation of ionospheric day-to-day variability by using  
37 GPS and Incoherent Scatter Radar observations, *Annales Geophysicae*, 25(8), 1815–1825, doi:10.5194/angeo-25-1815-2007,  
38 2007.